The Flying Saucer Concept for Micro Aerial Vehicles: Experimental Study

João Pedro Reis Rodrigues
joao.reis.rodrigues@tecnico.ulisboa.pt

Instituto Superior Técnico, Lisboa, Portugal

October 2021

Abstract

In this dissertation, an experimental study is presented regarding an innovative rotating disc wing, in an attempt to determine the viability of such a design in an application for micro aerial vehicles. A prototype was developed with two independently rotating convex discs, with a diameter of 400 mm and a relative thickness of 12%. Three rotation configurations were tested in a wind tunnel. The tests were performed at a Reynolds number of 100000, in a range of angles of attack from -2º to 20º, with a variation of Advance Ratio (AdvR), the ratio between disc edge speed and incoming flow speed, from 0 to 4 for synchronous rotation and fixed at 2 for the remaining cases. Additional flow visualization tests were performed for the synchronous rotation case at a specific range of angles and AdvR. Synchronous rotation indicated a better performance of the prototype at AdvR=2, given the lower values of drag and the small difference between lift values at different AdvR. This is due to a minimization of the separation bubble with turbulent structures of moderately small thicknesses. Asynchronous rotation with a static lower half suggests an increase in the generation of lift with the addition of rotating discs, since these values are larger than the fully static case, but smaller than the synchronous rotation one. Results for opposite rotations indicate a more significant influence of the bottom disc in the rolling moment, with the overall yaw moment approximately cancelling out.
Keywords: Rotating Disc Wing, Micro Aerial Vehicles, Wind Tunnel, Flow Visualization

1. Introduction

The concept of an aircraft with a "Flying Saucer" shape has been present in humanity's imagination since the midway point of last century. Prompted by the surge of so-called Unidentified Flying Objects (UFO) sightings, as well as through the representation of said aircraft in all forms of science fiction media, several engineers and researchers have been fascinated by the idea of converting these works of fiction into real, practical applications. As such, several studies have been made on circular wings and their feasibility, both in terms of generated aerodynamic forces and aircraft stability and control. One of the most recognizable prototypes that went past the design phase is Avro Canada's VZ-9AV Avrocar, a manned aircraft with circular wing that used the exhaust from turbojet engines to drive a circular "turborotor" which produced thrust. By directing this thrust, lift could be generated and some level of control could be achieved. The aircraft proved that the concept was possible, however, concerns about aerodynamic stability and increasing costs, led to the project being cancelled in December of 1961 [8].

However, the rise of interest in the Unmanned Aerial Vehicle (UAV), in particular the smaller platforms, of recent years has provided a renewed interest in the Flying Saucer concept. The All Directions Flying Object (ADIFO) prototype arose from such circumstances, offering a small Vertical Take-Off and Landing (VTOL) platform with unique aerodynamic features (such as a high lift-to-drag ratio and a smooth transition from subsonic to supersonic flight) and incredible manoeuvrability, due to its shape and use of multiple thrust nozzles [1].

Micro Aerial Vehicles (MAVs), which are categorized as autonomous flying vehicles with size restrictions, offer tremendous versatility, being used in all sorts of military, civilian and recreational activities. For the specific application in the military branch, the greatest advantage of these MAV is their capability for stealth, mainly due to their small size. As such, the use of the saucer shape in a MAV prototype could further increase its stealth capabilities, due to being a shape difficult to detect on radar and to the elimination of the rotor blades (responsible for the characteristic noise associated to these drones). Additionally, given that these

blades are considerably fragile components of these vehicles, removing them increases the robustness of the MAV. This factor is quite relevant, since the small size and high manoeuvrability of an MAV makes it a very adequate candidate for information gathering missions, in both military and civilian fields, sometimes in tight spaces where a larger platform could not operate. It is then inevitable that a MAV in this scenario is susceptible to damage and therefore it is important to be sufficiently robust to finish the mission even when hit by debris.

2. Background

In order to fully comprehend the obtained results of the aerodynamic study on the prototype, it is important to highlight some concepts and theories that lay the foundation for this work.

2.1. Basic Concepts

As with any other wing, the prototype will have a centre of mass, where the force of gravity acts on the body, as well as a centre of pressure, the point where all aerodynamic forces are applied. The two centres do not have to coincide with one another, with the centre of pressure being usually ahead (i.e. closer to the leading edge) of the centre of mass, for a Frisbee-like shape at typical flight angles of attack (AoA), as was summarized by Potts and Crowther [9].

A value that needs to be defined, being crucial for this study, is the advance ratio (AdvR). It is a measure of the edge speed of a disc in relation to the incoming flow speed and can be calculated as

$$AdvR = \frac{\Omega r}{U_\infty} \ , \tag{1}$$

where Ω and r are the rotation speed and radius of the disc, respectively, and U_∞ is the incoming flow speed. It is a commonly used ratio in rotating disc studies since it provides a dimensionless measure of the disc's rotation: if its value is equal to zero, the disc is static; if equal to 1, the edges of the disc are moving at the same speed as the incoming flow; if larger than 1, then the edges of the disc are moving faster than the free flow.

One of the objectives of this thesis is to analyse the aerodynamic forces generated by the developed prototype. There are three to consider, one for each Cartesian axis: the lift force, acting on the vertical axis; the drag force, acting on the horizontal axis parallel to the incoming flow; and the side-force, acting on the horizontal axis perpendicular to the incoming flow. In reality, this final force has a very small contribution to the overall aerodynamic behaviour of the prototype, with the first two being considerably more relevant to this study.

To explain it simply, lift is generated in any wing-like body due to its shape: the idea is to utilize a principle of conservation to force the flow going over the wing to be faster than the one going under it, by making the flow cover a longer distance on the top side. According to Bernoulli's principle, faster moving air is associated to lower pressures, meaning that a pressure gradient will appear, responsible for the generation of a force perpendicular to the flow, commonly known as lift. This force will increase with the AoA up to a critical angle, from there decreasing rapidly. This is what is commonly referred to as stalling. As for drag, it is a force parallel to the flow that opposes the movement of the wing, being always present as long as the wing is moving.

Since these forces act on the centre of pressure, they will cause the prototype to experience moments in relation to its centre of mass: a pitching moment around an horizontal axis perpendicular to the free flow, a rolling moment around an horizontal axis parallel to the flow, and a yaw moment around a vertical axis. These moments define the stability of the prototype in-flight, so their analysis is important to determine the performance of the discs.

If you consider an upwards lift force applied on the centre of pressure of a rotating disc, it will produce a nose-up pitching moment around the centre of mass. Since this moment is perpendicular to the angular momentum, a rotational property which has the same direction as the rotation speed of the disc, it will not change its magnitude, only its direction. This change is known as gyroscopic precession, being a critical phenomenon to the flight stability of a rotating disc. So in short, this precession consists of the axis of rotation moving towards the direction of the applied moment. In the described example, the pitching moment would be then translated into a rolling moment.

2.2. Laminar Separation Bubble

It is important to state that MAVs, on which the results from this study might be applied to, usually fly at a value of Reynolds number $Re < 200000$. Flying at this low Reynolds number is inevitable, considering the small size of these vehicles, which implies the appearance of certain phenomena associated to this type of flight, namely one known as laminar separation bubble.

A laminar boundary layer is highly susceptible to separation under adverse pressure gradients, since it

lacks the momentum transfer from turbulent mixing. When the layer separates from the surface, it forms a laminar and considerably unstable free shear layer. That promotes a transition, which leads to a high mixing and momentum transport, typically associated to turbulent flow, which allows for the flow to reattach itself to the surface. A fully turbulent boundary layer then continues past the reattachment point. A region with recirculating flow can be seen between the separation and reattachment points, known as the laminar separation bubble. This bubble is then responsible for a severe cut in aerodynamic performance, since drag increases and stability is reduced [10, 3].

2.3. von Kármán's Problem

In order to fully understand the type of flow that is seen over the prototype, it is important to mention what is commonly known as von Kármán swirling flow. This problem, solved by Theodore von Kármán in 1921, consists of an infinite rotating planar disc immersed in a still flow, where the rotation of said disc is the only contribution to setting the flow in motion. It is expected that a thin three-dimensional boundary layer is formed, due to the no-slip condition. The flow should be pushed outwards, due to the centrifugal force, and therefore be drawn axially so that mass conservation can be satisfied, as can be seen by the mean velocity profiles in figure 1, where the blue profile represented by U is the radial component, the red profile represented by V is the azimuthal component and the green profile represented by W is the axial component. Since the prototype consists of two discs, it is expected that a contribution of this type of flow is seen, once rotation is introduced.

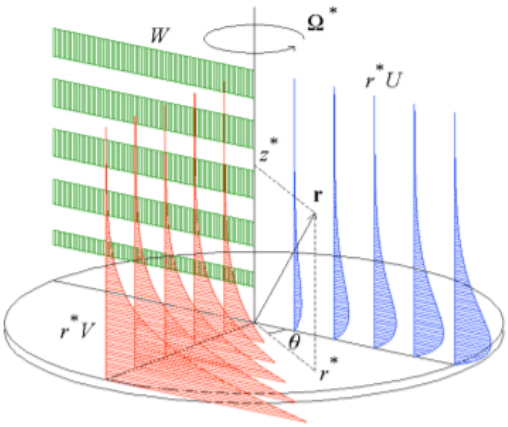

Figure 1: Sketch of the von Kármán boundary layer on a rotating disc showing the mean velocity profiles (in a stationary laboratory frame) [6].

3. Implementation

The design and execution of the prototype is of extreme importance, since it will provide the results to be analysed. As such the chosen concept should allow for the study of the effects of the rotation of the discs, with a minimum of aerodynamic interference in the results.

3.1. Conceptual Design

The design process produced several concepts, with a final decision being made on what was called design "epsilon". The key element of this epsilon configuration is then a central pillar that crosses the entirety of the prototype. Since this element is fixed, attaching a central platform (which will act as a base for the motors necessary to rotate the discs) to it means that one can ensure that this is also fixed, something that can be useful when operating the prototype, and which was difficult to ensure in previous designs. Additionally, the pillar can act as an alignment tool, guaranteeing the proper placement of all elements of the prototype during testing, as well as providing an easy way to implement the electric cables that will deliver power to the motors, with these going through the inside of it, as an hollow tube is being used.

A gear system is implemented to make the connection between the motors and the discs. Due to them being perpendicular to one another, the system was originally thought as a set of bevel gears, with the ones aligned with the central pillar needing to be hollow, in order to accommodate it. Additional ball bearings are placed on the pillar, not only to ensure a smooth interaction between the rotating discs and the static pillar, but also to fix the discs in their correct vertical positions.

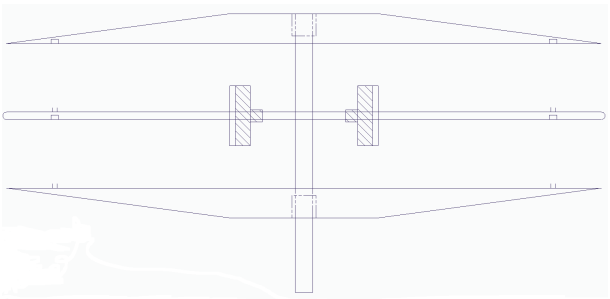

Figure 2: Sketch of the epsilon configuration.

3.2. Prototype's Characteristics

Several changes had to be made and more parameters defined, in order to turn this design into a functioning prototype. In terms of its profile, a diameter of 400 mm and a relative thickness of 12% were selected, to ensure a full immersion

in the incoming flow and to keep it as a slender profile. A symmetrical, biconvex shape was chosen, with its sharper edges aligning themselves with the study done by Kamaruddin [7], which should lead to a more aerodynamically efficient prototype. The central platform of the design was shortened to the necessary area to fix the two motors, which are now assembled horizontally. Due to that, the gear system was changed to a more simple set of spur gears. A "rail" system was implemented on the periphery of the discs, to act as an obstacle to the incoming air flow, preventing it from entering the prototype, as well as a base for a Polytetrafluoroethylene (PTFE) tube, which minimizes friction between the two discs.

3D printing was seen as the best manufacturing method for this work, given its quick production times and relatively low costs. A quick study on the mechanical properties of the materials to use, led to the decision of using Acrylonitrile Butadiene Styrene (ABS) for the central platform and Polylactic Acid (PLA) for the discs.

4. Results

The built prototype was tested in the open circuit wind tunnel located at the Mechanical Engineering Department of Instituto Superior Técnico. To allow for a wide range of AdvR in the tests, these were performed at the relatively low Reynolds number, $Re = 100000$. All results were obtained from "AeroIST", a previously developed software by Roque [11], as part of his Master's thesis. The forces and moments of the support making the connection between the aerodynamic scale and the prototype were measured and subtracted from the relevant obtained results. A correction on all lift-dependent coefficients was performed, based on the findings of Delgado [4]. The overall uncertainties associated to each of the coefficients were estimated based on the method described by Coleman and Steele [2]. Three types of rotation were tested and flow visualization images were obtained, to better understand the flow surrounding the prototype.

4.1. Synchronous Rotation

Tests with synchronous rotation of both discs were performed for AdvR equal to 0, 0.5, 1, 2, 3 and 4, in a range of AoA (represented by the greek letter alpha, α) from -2º to 20º. The plots from all relevant aerodynamic coefficients of this set of tests are presented from figure 3 to figure 7. Due to clearly dubious results, the plot in figure 6 does not contain the results regarding AdvR equal to 0.5 and 3. The calculated uncertainties are represented on the plots for two sets of AdvR results: AdvR=1 and AdvR=3 (or AdvR=4 in the case of figure 6).

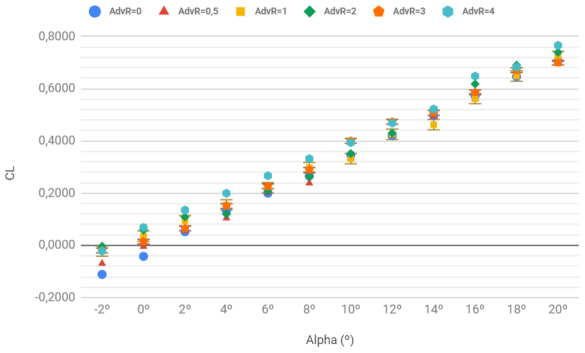

Figure 3: Lift coefficient results for the synchronous rotation tests.

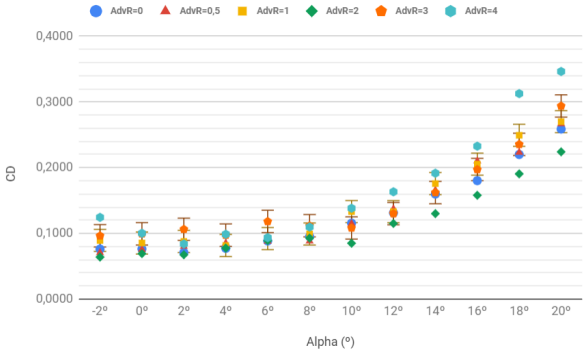

Figure 4: Drag coefficient results for the synchronous rotation tests.

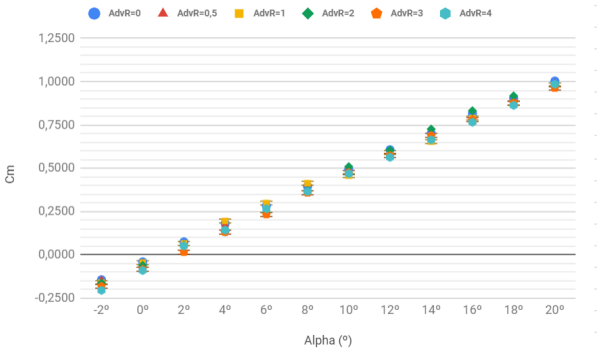

Figure 5: Pitching moment coefficient results for the synchronous rotation tests.

4.2. Asynchronous Rotation with Static Lower Half

Tests with asynchronous rotation, where the bottom disc is static, are performed. Unfortunate dimensional inaccuracies in the manufacture of the prototype led to significant oscillations between the discs in the asynchronous rotation tests, which limited the maximum AdvR value to be equal to 2. As such all results were obtained at this value and compared to the results of the same AdvR for the synchronous rotation.

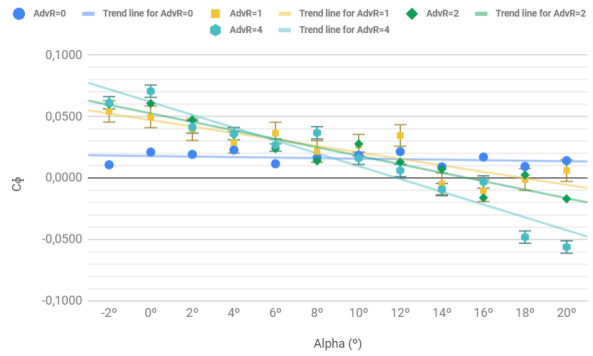

Figure 6: Roll moment coefficient results for the synchronous rotation tests.

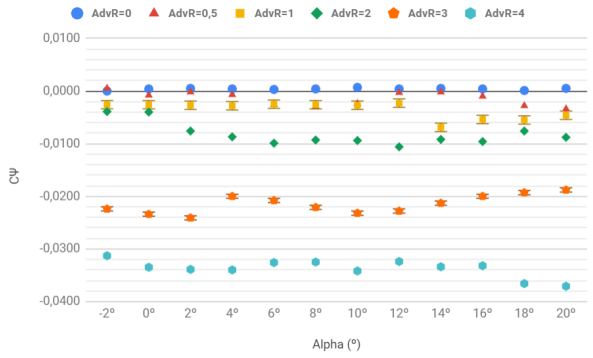

Figure 7: Yaw moment coefficient results for the synchronous rotation tests.

The plots from all relevant aerodynamic coefficients of this set of tests are presented from figure 8 to figure 11. In this case, the calculated uncertainties are presented in all of the obtained results. For a better analysis, figure 8 includes the results of AdvR=0 from the synchronous rotation tests.

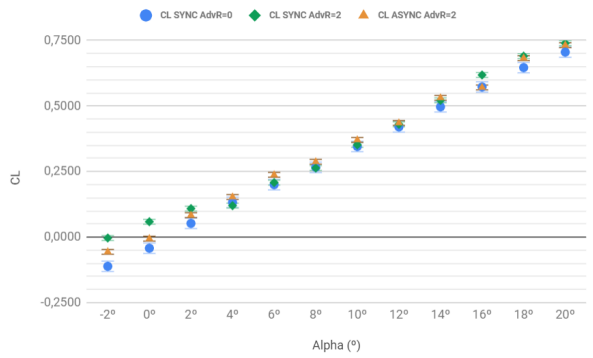

Figure 8: Lift coefficient results for the asynchronous rotation with static lower half tests.

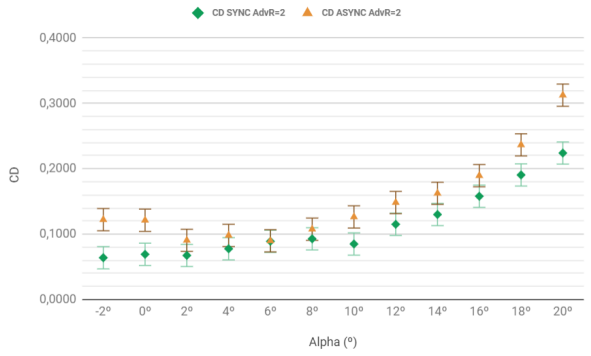

Figure 9: Drag coefficient results for the asynchronous rotation with static lower half tests.

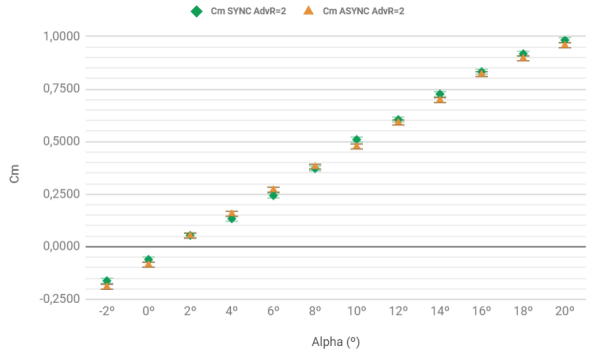

Figure 10: Pitching moment coefficient results for the asynchronous rotation with static lower half tests.

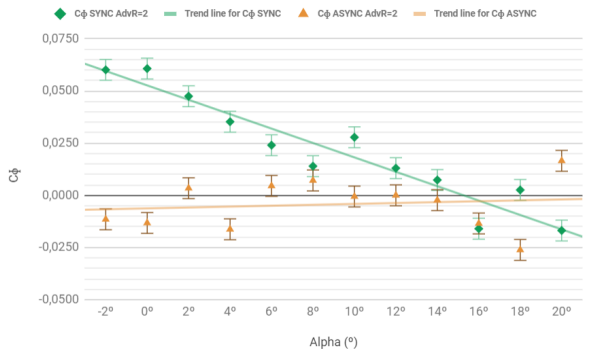

Figure 11: Roll moment coefficient results for the asynchronous rotation with static lower half tests.

4.3. Asynchronous Rotation with Opposite Directions

Final asynchronous rotation tests were performed, this time with both discs rotating at the same speed, but with opposite directions. A similar situation to the one described in subsection 4.2 is also present in this set of tests, as such they were performed at an AdvR=2 and compared to the synchronous rotation results at that AdvR value. The plots with the relevant aerodynamic coefficients are then presented

from figure 12 to figure 16, with the calculated uncertainties being presented in all results once more.

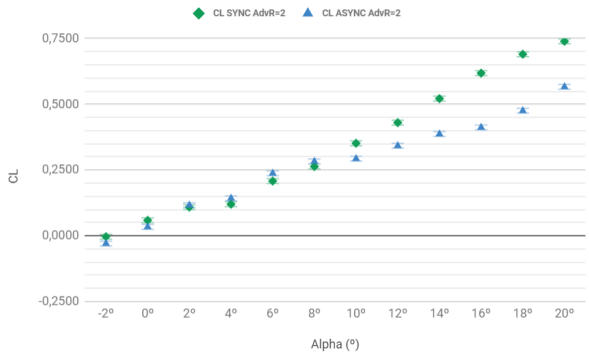

Figure 12: Lift coefficient results for the asynchronous rotation with opposite directions tests.

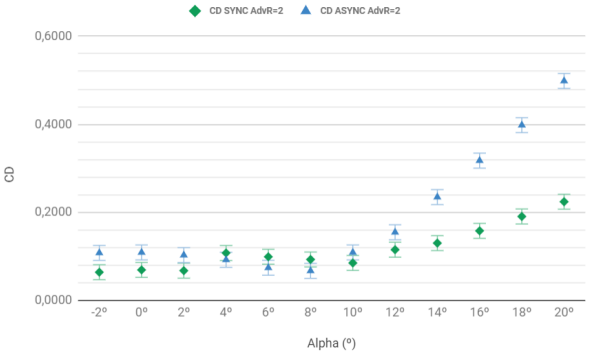

Figure 13: Drag coefficient results for the asynchronous rotation with opposite directions tests.

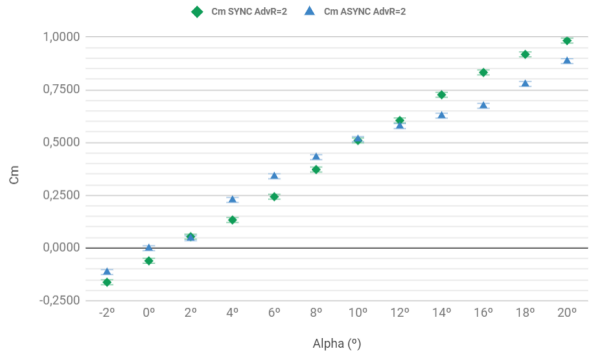

Figure 14: Pitching moment coefficient results for the asynchronous rotation with opposite directions tests.

4.4. Flow Visualization

To better understand the flow behaviour surrounding the prototype, a system typically used for particle image velocimetry (PIV) tests was used to obtain qualitative flow visualization images over the

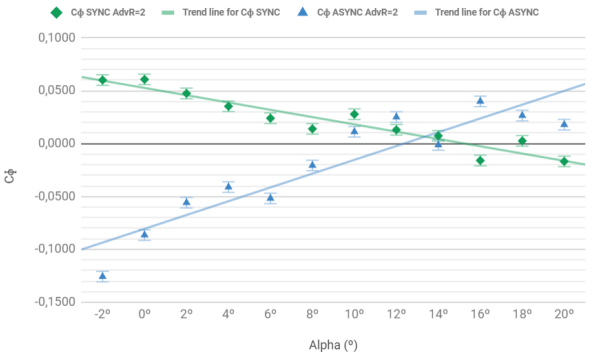

Figure 15: Roll moment coefficient results for the asynchronous rotation with opposite directions tests.

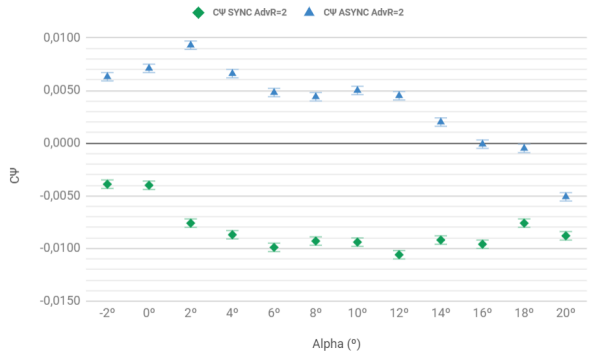

Figure 16: Yaw moment coefficient results for the asynchronous rotation with opposite directions tests.

top disc. Some AoA and AdvR values were selected to represent the entire range of the performed tests: two low AoA (0^o and 4^o), one medium AoA (10^o) and one high AoA (20^o), no rotation (AdvR=0), medium rotation (AdvR=2) and high rotation (AdvR=4). In order to obtain as clear of an image as possible, the configuration that offered the least amount of oscillations, i.e. the one used in subsection 4.1 was used. The results are displayed from figure 17 to figure 20.

4.5. Analysis of Results

Beginning the analysis with the flow visualization images at an α=0^o (figure 17): it can be clearly seen that, without rotation, there is a separation of the boundary layer as soon as an adverse pressure gradient begins to appear (at 50% of the chord). This is due to two factors, the first being the geometry of the prototype itself, which induces said pressure gradient. The second is the relatively low Reynolds number at which the tests were performed, indicating a laminar boundary layer, which is much more susceptible to separation than a turbulent one associated to higher values

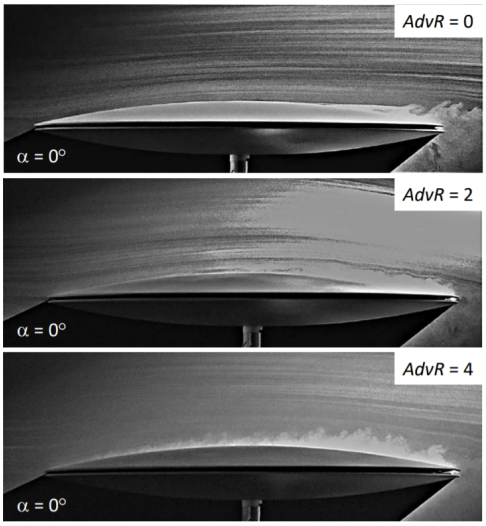

Figure 17: Flow visualization for α=0º.

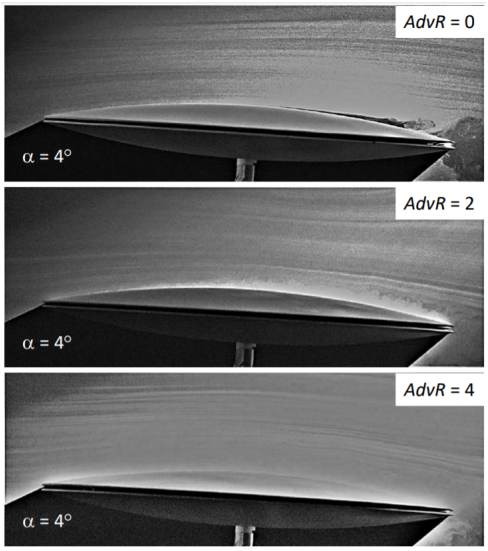

Figure 18: Flow visualization for α=4º.

of the Reynolds number. Introducing rotation on the discs leads to an interaction between the induced von Kármán flow and the already present horizontal flow, which creates some turbulent structures. At an AdvR=2, these begin roughly at the midpoint of the chord, with the boundary layer section between the leading edge and that point presenting laminar flow characteristics. Crucially however, the introduction of the turbulent structures triggered a transition of the boundary layer, suppressing its separation. The increase of rotation to AdvR=4 simply led to the turbulent structures beginning closer to the leading edge, seen by the clear earlier transition of the boundary layer.

At an α=4º (figure 18), the case of AdvR=0 is very similar to the previous one: there is still a

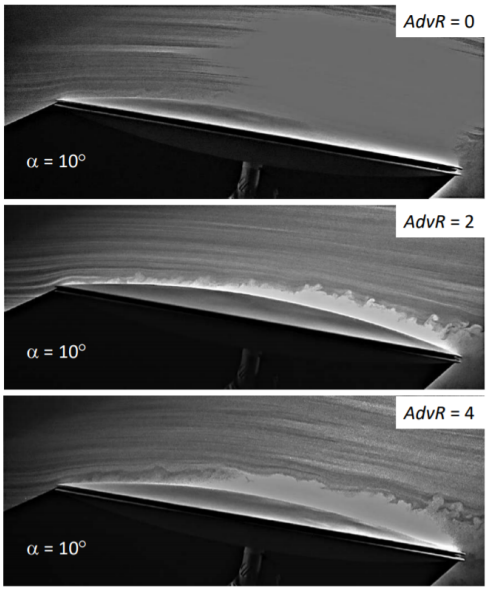

Figure 19: Flow visualization for α=10º.

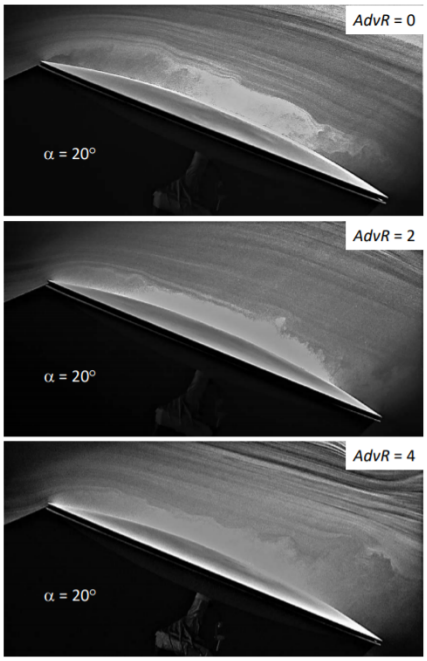

Figure 20: Flow visualization for α=20º.

laminar separation of the boundary layer, albeit happening slightly closer to the leading edge, due to the increase in AoA. In the case of AdvR=2, it is once again clear that the addition of rotation led to the creation of turbulent structures which prevent the separation of the boundary layer. This time however, transition begins much closer to the leading edge, being more comparable to the case of AdvR=4 at the previous AoA. This can be simply explained as an outcome of the increased AoA as well as the sharp edges of the prototype which will

increase the air flow speed over the surface of the prototype, also increasing the Reynolds number, which of course triggers an earlier transition. At an AdvR=4, despite the lack of clarity in the picture, an increase of the thickness of the turbulent boundary layer can be observed.

Moving on to an α=10º (figure 19), at an AdvR=0 it can be seen that a small separation bubble is present near the leading edge. This can be explained by the fact that, at this angle, the sharp edge will increase the flow speed to a point that can not be maintained following the leading edge. This effectively means that a considerable adverse pressure gradient exists in that area, forcing the flow to separate. However, the relatively low Reynolds number of the incoming air flow allows the separated flow to "mix" with it, leading to an increase of turbulence which promotes the flow to reattach to the surface of the disc aft of the leading edge, this time forming a turbulent boundary layer, which prevents further separation. The addition of rotation at AdvR=2 leads to a forced transition which triggers the appearance of turbulent structures closer to the leading edge, however the separation bubble is still present, with the separated flow reattaching roughly at the same point. Despite that, it is clear that the thickness of the boundary layer is considerably larger, no doubt due to the interaction with the von Kármán swirling flow. Increasing to an AdvR=4, it is clear that there is an increase in the thickness of the boundary layer, which is in-line with what has been found up to this point.

Finally, analysing the images taken at α=20º, it can be seen that without rotation, the flow separates right at the leading edge, quickly transitioning into turbulent flow. It then reattaches to the surface of the disc somewhere near the midpoint of the chord. At an AdvR=2 the separation is still clearly visible, however, the added rotation has clearly decreased its thickness. Increasing the rotation to an AdvR=4 does not seem to affect the separation bubble any further, however, an increase of the thickness of the turbulent structures is verified, as is expected.

In terms of the plots of the aerodynamic coefficients, let us begin by analysing the ones regarding the tests with synchronous rotation:

- C_L **(figure 3):** it can be seen that the slopes $\left(\frac{\partial C_L}{\partial \alpha}\right)$ for the different AdvR results remain approximately constant. The values for AdvR=4 seem to be consistently above all other values, which is in-line with what CFD simulations done by Gomes [5] suggest that a very small increase should be expected at this AdvR. A note can be made regarding the dispersion of values, which is considerably larger at lower AoA. This can be explained simply by the fact that, at lower AoA, the generated forces are smaller, being naturally more difficult to measure accurately. As the AoA is increased so too are the generated forces, leading to a smaller dispersion between all AdvR;

- C_D **(figure 4):** for most AdvR, the values seem to be approximately the same, however, there are two exceptions. The first one is for AdvR=2 where it can be verified that the obtained values are generally lower, particularly at higher AoA. This aligns itself with what was observed in the flow visualization images, since it was at this value that some of the separation bubbles could be suppressed and, crucially, the turbulent structures were kept at moderately small thicknesses. Both of these factors contribute to an expected lower drag force, which is seen on the plot. The second exception is for an AdvR=4, with clearly larger values, that can be explained by the considerable thickness of the turbulent structures. Despite the fact that most of the verified separation bubbles can be suppressed at this AdvR, the size of the turbulent vortices that are formed leads to a considerable increase in drag, an effect which is logically more noticeable at higher AoA, since it is paired up with the existence of the unsuppressed separation bubbles;

- C_m **(figure 5):** within the expected, with the results approximately equal across all tested AdvR values, a logical result if one takes into consideration the CFD results for C_L, since the pitching moment is directly dependent of this variable;

- C_ϕ **(figure 6):** it becomes clear that the rotation of the discs has an impact in this coefficient. Given how for an AdvR=0 the obtained values are approximately equal to zero and constant, with all other AdvR presenting different values, it can be concluded that the aerodynamic centre is located on the longitudinal symmetry axis of the prototype without rotation, being moved away from said axis with the introduction of rotation. Also of note is the gyroscopic effect present with the rotation of the discs, which certainly contributes for the noticeable difference between all AdvR results;

- C_ψ **(figure 7):** presents expected values, with an observable increase in the yaw moment from an AdvR=2 onward, when rotation

begins to be more intense.

As for the analysis of the asynchronous rotation plots, beginning with the case of the fixed bottom disc:

- C_L **(figure 8):** it can be seen that, although the difference between the values is relatively small, the results of the asynchronous rotation are roughly located between the synchronous rotation values taken at AdvR=0 and AdvR=2. This suggests that having two rotating discs is more beneficial than just one, in terms of lift generation, however, it also becomes clear that, for this prototype, having a single disc in rotation creates more lift than two static discs;

- C_D **(figure 9):** the asynchronous rotation can be observed to have, in general, larger values of C_D, indicating the possibility of it not enjoying the effect responsible for the lower values on the synchronous rotation case, described previously. This, however, is not within the expected, since the top disc is still rotating in the asynchronous case and therefore should be generating the mentioned effect. A possible explanation is that the added oscillations present in the asynchronous rotation led to an increase of the thickness of the turbulent structures on the top disc, which led to an increase of drag.

- C_m **(figure 10):** despite not showing a large difference between asynchronous and synchronous rotations, the plot suggests a trend between the results similar to what is seen for the C_L values, which is within the expected;

- C_ϕ **(figure 11):** Despite considerable oscillations, an analysis of the trend line of the results seems to indicate a decrease in this coefficient for the asynchronous rotation case. This can be explained by the decrease of gyroscopic effects, since now one of the discs is immobilized.

Finally, the case of asynchronous rotation with opposite rotation directions:

- C_L **(figure 12):** results indicate a clear decrease in lift for the asynchronous rotation, particularly at higher AoA, not at all within what is expected, given how the direction of the rotation of the discs should not influence the amount of lift that is generated;

- C_D **(figure 13):** these results may help to clarify the behaviour of C_L, since an increase in drag is verified, once again being more noticeable at higher AoA. This suggests the presence of larger turbulent structures and even a larger separation bubble, no doubt a possible outcome of the considerable oscillations that were visually perceived between the discs during these tests;

- C_m **(figure 14):** results follow the same trend as the ones from C_L, as would be expected;

- C_ϕ **(figure 15):** an analysis of the trend line clearly indicates results with opposite signs to those obtained from the synchronous rotation case, which could indicate that the bottom disc has a larger contribution for this coefficient, since it was the one that changed the direction of rotation. This explanation also aligns itself with the values for this variable with a static bottom disc;

- C_ψ **(figure 16):** despite some oscillations, these results seem to be closer to zero for the asynchronous rotation, an expected outcome given how the discs should produce yaw moments with opposite directions but in equal magnitude.

5. Conclusions

A prototype was conceptualized and built to allow for the study of the impact of rotation on the aerodynamic performance of a circular wing. The prototype, made from PLA and ABS through a 3D printing manufacturing method, allows for the independent rotation of its two constituting discs.

Aerodynamic forces and moments were obtained from three types of tests: synchronous rotation of the discs, in the same direction; asynchronous rotation, with the bottom disc immobilized; same speed asynchronous rotation, with the discs rotating in opposite directions. Qualitative flow visualization images were obtained for the synchronous rotation case.

Flow visualization images suggest the appearance of a separation bubble beginning at AoA=10^{o}, which grows in size with increase of AoA. The introduction of rotation produces a von Kármán swirling flow which then interacts with the incoming flow from the tunnel, triggering the appearance of turbulent structures which help to suppress the separation bubble. An increase of AdvR is shown to lead to a larger suppression of the bubble, as well as an increase in the thickness of the turbulent structures. A more in-depth flow visualization study, which should include a quantification of the flow field using PIV, is recommended to better

understand the surrounding flow on all of the prototype's configurations.

Results from the synchronous rotation tests indicate a slight increase of the lift coefficient for an AdvR=4. Drag coefficient values are lower for an AdvR=2, a result of the minimization of the separation bubble without turbulent structures of large thickness. That, together with the proximity of the lift coefficient results for all AdvR, indicates a better aerodynamic performance at this specific AdvR. Roll moment coefficient results suggest a change of position of the aerodynamic centre, as well as the presence of gyroscopic effects, with the introduction of rotation.

From the asynchronous rotation with a static lower half tests, it can be seen that lift increases with the addition of a rotating disc, being proportional to the number of discs in rotation. Roll moment coefficient values decreased, due to a reduction of gyroscopic effects.

As for the asynchronous rotation with opposite directions results, a decrease in aerodynamic performance (less lift with more drag) is verified at higher AoA, due to the considerable oscillations between the discs, an outcome of the unfortunate dimensional inaccuracies in manufacture. Roll moment coefficient values indicate a change in sign across the AoA range, when compared to the synchronous rotation case, suggesting a larger influence of the bottom disc on this coefficient, since it was the one changing its direction of rotation. Yaw moment coefficient results show a decrease, when compared to the synchronous rotation case, an expected outcome given the discs should be producing yaw moments with opposite directions.

The range of tested AdvR became quite limited, especially in regards to the asynchronous rotation tests, an outcome of the aforementioned dimensional inaccuracies. As such, a rebuild of the prototype is suggested, with special care given to the dimensional accuracies being respected during the manufacturing process. This should allow for a larger range of AdvR to be tested, as well as more stable results to be obtained. Given the results of this study, it seems relevant to further investigate this concept, making it a worthwhile investment.

Acknowledgements

I would like to thank Prof. João Manuel Melo de Sousa, for his irreplaceable support throughout the development of this work, with his expertise, readiness to help and contagious enthusiasm for the project.

A special thank you to my friends and family who have helped me to keep moving forward towards my goals, being the lights illuminating the path which led me here.

References

[1] ADIFO Aircraft. ADIFO. http://www.adifoaircraft.com/. Accessed: 2020-11-25.

[2] H. W. Coleman and W. G. Steele. *Experimentation, validation, and uncertainty analysis for engineers*. John Wiley & Sons, 4th edition, 2018.

[3] V. de Brederode. *Aerodinâmica Incompressível: Fundamentos*. IST Press, 1st edition, 2014.

[4] H. Delgado. *Novas Tecnologias Biomiméticas para a Aerodinâmica de Veículos Aéreos a Baixo Número de Reynolds*. PhD thesis, Instituto Superior Técnico, 2018.

[5] M. Gomes. The flying saucer concept for micro aerial vehicles: Computational study. Master's thesis, Instituto Superior Técnico, July 2021.

[6] S. Imayama. Experimental study of the rotating-disk boundary-layer flow. Technical report, Royal Institute of Technology, 2012.

[7] N. M. Kamaruddin. *Dynamics and Performance of Flying Discs*. PhD thesis, School of Mechanical, Aerospace and Civil Engineering - University of Manchester, 2011.

[8] National Museum of the United States Air Force. Avro Canada VZ-9AV Avrocar. https://www.nationalmuseum.af.mil/Visit/Museum-Exhibits/Fact-Sheets/Display/Article/195801/avro-canada-vz-9av-avrocar/, 2015. Accessed: 2020-11-25.

[9] J. Potts and W. Crowther. $Frisbee^{TM}$ aerodynamics. *20th AIAA Applied Aerodynamics Conference Exhibit*, June 2002.

[10] W. B. Roberts. Calculation of laminar separation bubbles and their effect on airfoil performance. *AIAA Journal*, 18(79-0285R), 1980.

[11] F. Roque. Desenvolvimento de uma plataforma aberta e escalável para aquisição de dados no túnel aerodinâmico de baixa velocidade. Master's thesis, Instituto Superior Técnico, Oct. 2012.